

RSC Advances



This is an *Accepted Manuscript*, which has been through the Royal Society of Chemistry peer review process and has been accepted for publication.

Accepted Manuscripts are published online shortly after acceptance, before technical editing, formatting and proof reading. Using this free service, authors can make their results available to the community, in citable form, before we publish the edited article. This *Accepted Manuscript* will be replaced by the edited, formatted and paginated article as soon as this is available.

You can find more information about *Accepted Manuscripts* in the [Information for Authors](#).

Please note that technical editing may introduce minor changes to the text and/or graphics, which may alter content. The journal's standard [Terms & Conditions](#) and the [Ethical guidelines](#) still apply. In no event shall the Royal Society of Chemistry be held responsible for any errors or omissions in this *Accepted Manuscript* or any consequences arising from the use of any information it contains.



Journal Name

ARTICLE

Synthesis, characterization of carbon micro tube/tantalum oxide composites and their photocatalytic activity under visible irradiation†

K. Chennakesavulu^{a,b*} and G. Ramanjaneya Reddy^c

Received 00th June 20xx,
Accepted 00th June 20xx

DOI: 10.1039/x0xx00000x

www.rsc.org/

The carbon microtubes (CMTs) was synthesized by combustion of cotton fibers in open air atmosphere at optimized temperature. The combustion of cotton fibers leads to the formation of CMTs by self rolling approach. Insitu synthesis of CMT:Ta₂O₅ composite was done in alkaline ethanolic medium. The formation of CMTs and composites were characterized by the RAMAN, DRS/UV-Visible, FTIR, XPS, XRD, BET, N₂-adsorption isotherms, FESEM/EDX, TEM/EDX and Particle size analysis. The composites were effectively employed in the photo oxidation of xylenol orange (XO) and methyl orange (MO). The composites catalytic activity and adsorbed dyes removal percentage were determined by the spectrophotometric method. The CMT:Ta₂O₅ composites ascertained higher photocatalytic activity due to the nascent oxygen enhances the photocatalytic performance. The kinetic parameters obey *pseudo*-first order reaction, it may be due to the constant amount of the catalyst and concentration of dye solution. The catalytic activity of the recycled composites was compared with the fresh catalyst.

Introduction

Carbon microtubes are new form of carbon, in addition to more conventional forms such as graphite, diamond, fullerenes, carbon nanotubes (CNTs), carbon nanospheres, mesoporous carbon, carbon micro coils and carbon nanofoams. The CNTs are rolled graphene layers having diameter less than 1 μm. The synthesis of CNTs and their applications are widely investigated. But, the disadvantage of the CNTs is commercial availability in large quantity in required diameter, dispersion, solubility of the CNTs in aqueous medium. The functionalization of CNTs with proteins, cells, inorganic clusters also a tedious process. In spite of more advantages of CNTs, the development of carbon based inexpensive, stable, efficient, band gap tunable surface active materials is still a major challenge. The CMTs have hollow tubular structure with diameter from 10 μm to 150 μm.¹ The CMTs can act as another

substituent to the CNTs. The CMTs synthesis and physio-chemical characterization needs to be established. In 1960s first the Roger Bacon from Union Carbide company reported the formation of graphite whiskers during the pyrolysis of carbon monoxide at 1800 °C.^{2,3} Microtubes can be applied in the fields of gas sensors and microfluidics. The CNTs fabrication methods such as arc discharge method and pulse laser ablation cannot be used to fabricate the carbon micro tubes (CMTs). The synthesis of CMTs was complex and time consuming process with larger diameter. The CMTs have the potential of becoming a key material in meso scale science. The CMTs were synthesized from natural renewable precursor (coconut oil) by chemical vapour deposition. The CMTs were synthesized in a nitrogen atmosphere at a temperature of 1175 °C and at a flow rate of 100 mL/min using ferrocene as catalyst.⁴ The CMTs were synthesized by carbonization of poly (acrylonitrile) fibers,⁵ catkins,⁶ bucky paper (Gas pressure enhanced CVD),⁷ activated carbon,⁸ reed bristles,⁹ propane,¹⁰ acetylene (PE-CVD),¹¹ fluff of chinar tree,¹² Urea,¹³ graphite,¹⁴ plant biomass,¹⁵ and polyvinyl butyral powder.¹⁶ The carbon /metal hybrid microtubes of very high aspect ratio via self-rolling approach of polymer multilayers. The microtubes are expected to have potential applications in areas such as micro fluidic devices and catalysis.¹⁷ Voloshini et al investigated the properties of virtual CMTs as function of their diameter and the number of atoms constituting a ring or a spiral turn of the microtubes. In order to describe the properties of CMTs they used first time evaluated by the electron density distribution method.¹⁸

^a Department of Chemistry, Sathyabama University, Sathyabama University, Chennai-600 119, India. Tel/Fax: +914424503814.

^b Centre for Nano Science and Nano Technology, International Research Centre, Sathyabama University, Chennai-600 119. Email: chennam1@yahoo.com

^c Department of Inorganic Chemistry, Guindy Campus, University of Madras, Chennai - 600 025, India.

† Electronic Supplementary Information (ESI) available: [The Particles size graphs, Cotton fiber powder XRD, Cotton FESEM/EDX, FESEM/TEM-EDAX spectral of composites, Pore volume graphs, Absorption plots of XO and MO. The Raman, DRS (smoothed) and XRD patterns of the recovered catalysts were given in the electronic supplementary information. See DOI: 10.1039/x0xx00000x

The carbon composites widely used in the field of catalysis, sensors, high thermal conductive materials, adsorbents for toxic metals and organic pollutants. In the field of catalysis the carbon composites with metal, metal complexes and metal oxides are widely reported.^{19,20} Silica/CNT coupled with metal oxides such as TiO₂, ZrO₂, Al₂O₃ and ZnO were also being used as photocatalysts.^{21,22} Relative to these oxides the tantalum and niobium oxides and their composites are having growing interest in various fields. Niobium oxide and tantalum oxide are good visible light absorbents and these oxides are potential catalytic materials for heterogeneous catalysis reactions and organic transformations.^{23,24} The Ta₂O₅ is good semiconducting material with a high dielectric constant and high index of refraction, which has found important applications such as Dental imaging, CT Scans and X-rays, coatings, plastics nanowires, textiles, nanofibers, alloys, catalyst applications and better material for the environmental pollutant water treatments.²⁵ The Ta₂O₅/TiO₂ photocatalyst was prepared by simple solid-solid reaction technique with different Ta:Ti ratios and used in the degradation of methylene blue.²⁶ Tantalum (oxy)nitrides were synthesized by the nitridation of Ta₂O₅ and were added to a photo-Fenton-like system to enhance Fe³⁺ reduction and atrazine degradation under visible light.²⁷ Ta₂O₅-IrO₂ thin film was used as the electrocatalyst in electrochemical degradation of lignin.²⁸ The graphene, Zn-Al-In mixed metal oxides/carbon nanotube composite shows high performance in photocatalysis. Even at lower CNT percentage was ascribed to the synergistic effects of supporting and electron-hole recombination and e⁻ trapping effect the transition metals.²⁹ The MWCNT reinforced ZnO composites were utilized as anode material for Li-ion batteries, microwave absorbing material, nanoresonators and ammonia sensor. The MWCNT decorated ZnO nano structures were used as photocatalytic, sonocatalytic and sonophotocatalytic degradation of rhodamine-B.³⁰ In-situ synthesis of ZnO:Ta₂O₅/Nb₂O₅ composites were used as photocatalysts in the degradation of chloro phenols, cationic and anionic dyes. The degradation of cationic, anionic, nonionic dyes are difficult under UV/Visible by carbon composite. Tantalum oxides could act as active catalyst with high surface area carbon materials. The carbon materials were used to minimize the electron-hole recombination besides relative number of active sites present on the surface of the heterogeneous catalyst.³¹ The synthesis of the conducting material like CMTs from the insulating cotton material by inexpensive and rapid process are yet to be reported. The composites of CMTs and tantalum oxides and their usages in photocatalysis under UV/Visible light also yet to be reported.

In the present investigation carbon source for CMTs is surgical cotton and the first approach to involve the open air atmosphere combustion of cotton to CMTs. This study reveals the synthesis of CMT and its composites by Ta₂O₅, which is precursor of tantalum chloride. The CMT:Ta₂O₅ composites formation with different ratio of tantalum oxide, was confirmed by various characterization techniques. The tantalum doped CMTs may restrict electron-hole recombination during the dye degradation Higher photocatalytic activity was observed for

CMT:Ta₂O₅ composites towards the removal percentage of XO and MO dyes when compared to that of CMTs. The optical absorption spectral studies are used to determine the photocatalytic activity and kinetic parameters. The reused catalysts photo catalytic activity was compared with that of fresh catalyst.

Experimental

Materials

Ammonia (Merck Pvt. Ltd, India), Xylenol orange tetra sodium salt, Methyl orange (Lobachemie, India), Tantalum penta chloride (Sigma-Aldrich Pvt. Ltd, India), Cotton fiber and other analar grade chemicals were used without further purification. Millipore water was used throughout the work.

Physicochemical measurements and characterization

The FTIR spectra were recorded on a FTIR Perkin-Elmer 8300 spectrometer with KBr disk. The UV-Vis absorption spectra of liquid samples were recorded on a Perkin Elmer Lambda-35 spectrophotometer. The UV-Visible Diffuse Reflectance Spectral (UV-Vis/DRS) analyses were carried out on a JASCO-V-670 UV-visible spectrophotometer. Raman spectra were recorded on a NANO PHOTON11i confocal Raman microscope using a He-Ne laser emitting at 532 nm. The crystalline nature of the CMT:Ta₂O₅ composites was ascertained by powder X-ray diffraction using Rigaku XRD-Smart Lab with Cu-Kα₁ radiation (λ=1.5418 Å). The N₂-adsorption, desorption isotherms and Brunauer-Emmett-Teller (BET) surface area measurements at -196 °C were carried out on a Micrometrics ASAP (Model 2020) surface area analyzer with nitrogen and helium gases with a purity of 99.99%. The FESEM was obtained on a FESEM-SUPRA 55-CARL ZEISS scanning electron microscope. The XPS analysis was carried out on XM1000 Omicron nanotechnology XPS system with Al-Kα monochromatic wavelength. The samples were made in to pellets and were used as such for X-ray photoelectron spectroscopic (XPS) studies. The high resolution XPS traces were deconvoluted using the Gaussian statistical analysis by using origin-7 software. The HRTEM analysis was carried out by using a FEI TECNAI G2 (T-30) transmission electron microscope with an accelerating voltage of 250 KV. The CILAS particle size analyzer model 1180 was used to measure the particle size of CMTs and their composites.

Preparation of the carbon microtubes

The known amount of cotton was well dispersed in glass tray. The cotton was allowed to burn for two to five minutes. During the combustion temperature was monitored by thermocouple, which was fixed to glass tray. Unexpectedly the CMTs formation was observed. The same method was repeated for five times and reproducibility was also confirmed. The combustion temperature was monitored to be at approx. 450 °C. During the combustion, cotton fibers rolled them self under differential aeration as results CMTs.

Preparation of the CMT:Ta₂O₅ composites

The tantalum chloride of 0.3 M was well dispersed in 200 mL of ethanol solution, in double neck round bottom flask, 1.2 M ammonia solution was added drop wise in above solution at room temperature and fixed amount of CMTs was added to this solution. The resulting solids was centrifuged and repeatedly washed with the milli-Q water. The black threads were heated in furnace at 300 °C for 4 h. The pure CMTs and composites prepared with 1%, 3% and 7% of tantalum oxide in CMTs were represented as CMT:Ta₁, CMT:Ta₂, CMT:Ta₃ respectively.

Photocatalytic degradation of the XO under visible light irradiation

The photo catalytic activities of the CMTs, CMT:Ta₁, CMT:Ta₂ and CMT:Ta₃ in removal of the XO under visible light in a cylindrical glass reactor with the each catalyst 0.1 g of CMTs, CMT:Ta₁/CMT:Ta₂/CMT:Ta₃ and 0.1 mmol of 100 mL aqueous dye solution was added to the catalysts separately. The reaction conditions are optimized in dark at room temperature and start irradiation under visible light (> 420 nm). The removal percentage and consequent spectral changes at predetermined time intervals were monitored by the UV-Visible absorption spectra at 436± 2nm for 4 h. The percentage conversion is calculated from equation (1).

$$A = \epsilon c l \quad (1)$$

Here, ϵ = molar extinction coefficient [$M^{-1} \text{ cm}^{-1}$], c = sample concentration, l = path length of cuvette (1 cm).

Photocatalytic degradation of the MO under visible light irradiation

The photo catalytic activities of the CMTs, CMT:Ta₁, CMT:Ta₂ and CMT:Ta₃ in removal of the MO under visible light in a cylindrical glass reactor with the each catalyst 0.1 g of CMTs, CMT:Ta₁/CMT:Ta₂/CMT:Ta₃ and 0.2 mmol of 100 mL aqueous dye solution was added to the catalysts separately. The reaction conditions are optimized in dark at room temperature and start irradiation under visible light (> 420 nm). The removal percentage and consequent spectral changes at predetermined time intervals were monitored by the UV-Visible absorption spectra at 464 ± 2 nm for 2 h. The percentage conversion is calculated from equation (1).

Results and discussion

RAMAN spectral studies

The Raman spectra of CMTs, CMT:Ta₁, CMT:Ta₂ and CMT:Ta₃ are shown in Fig.1. The peaks at 1330 cm^{-1} and 1573 cm^{-1} indicates the D-band and G-band respectively. The characteristic bands were also observed for the graphite and carbon nanotubes.³² The composites has the same structural integrity of CMT frame work. The peaks in the region of 110-480 cm^{-1} and 500-910 cm^{-1} were due to the presences of Ta₂O₅ in the composites, but this peaks were absent in case of pure CMTs. The peaks at 740 cm^{-1} and 870 cm^{-1} are due to the octahedral TaO₆ modes. The peaks at 410 cm^{-1} and 210 cm^{-1} indicates Ta-O units. The peaks at 465 cm^{-1} and 572 cm^{-1} indicate the terminal Ta-O bond vibrations. The peaks at 735-

821 cm^{-1} was due to the Ta₂O₅ moiety of composites. The Raman shift around 910 cm^{-1} was due to the stretching mode of the O=Ta-O-H bond vibration.³³ The Raman spectral analyses clearly suggest that the formation and stability of tantalum oxide with CMT frame work.

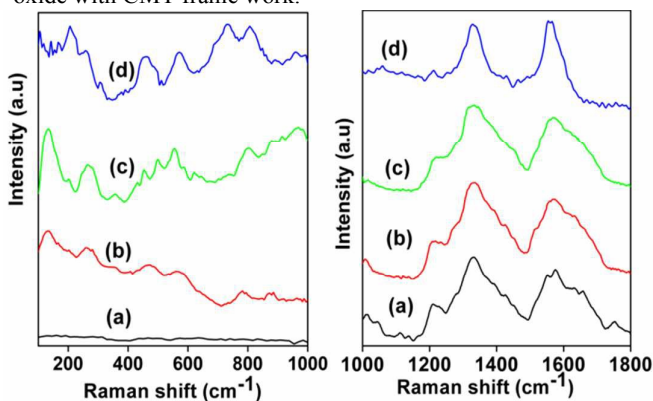


Fig. 1 Raman spectra of the (a) CMTs (b) CMT:Ta₁ (c) CMT:Ta₂ and (d) CMT:Ta₃

DRS/ UV visible spectral analysis

DRS/UV-visible spectra of the CMTs, CMT:Ta₁, CMT:Ta₂ and CMT:Ta₃ were shown in the Fig.2. It was found that the absorption spectra of the CMT and CMT:Ta₂O₅ were quite different. The CMTs show a peak at 236 nm, where as the CMT:Ta₂O₅ composites shows in the region of 310-335 nm and at higher percentage of the tantalum oxide a slight peak broadening was observed. The absence of peak in the region of 400-800 nm clearly indicates the tantalum has d⁰ configuration.³⁴

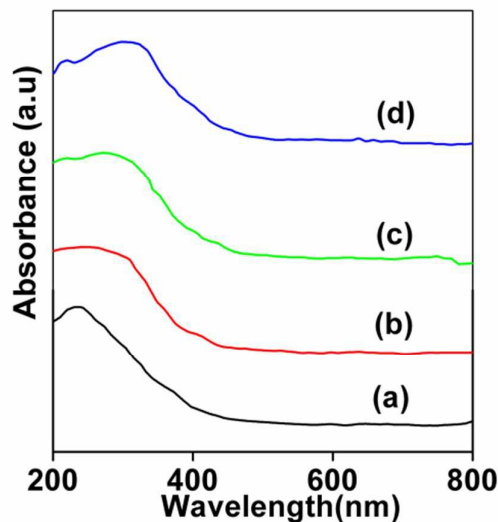


Fig. 2 DRSUV/Visible spectra of the (a) CMTs, (b) CMT:Ta₁ (c) CMT:Ta₂, (d) CMT:Ta₃

FTIR spectral analysis

Fig. 3. shows a typical FTIR spectra of CMTs, CMT:Ta₁, CMT:Ta₂ and CMT:Ta₃. The strong and broad peak around 3400 cm⁻¹, corresponds to the stretching frequency of O-H groups. The peak at 1638 cm⁻¹ was due to the in plane bending vibrations of the Ta-OH groups. The peak around 3500-3650 cm⁻¹ due to stretching vibrations of the HO-Ta=O(O₂H) units. The CMT:Ta₂O₅ exhibits peaks in the range of 450-1000 cm⁻¹ was due to the vibration modes of Ta₂O₅, but there is no peak

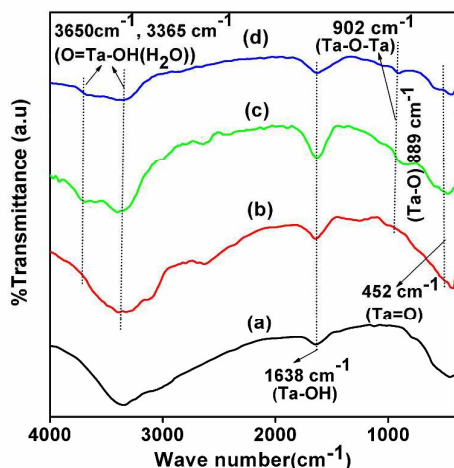


Fig. 3 FTIR spectra of the (a) CMTs (b) CMT:Ta₁ (c) CMT:Ta₂ and (d) CMT:Ta₃

for pure CMTs. The peaks at 890 cm⁻¹, indicates the Ta-O-Ta mode of vibrations. The peak at 452 cm⁻¹ was due to the T=O mode of vibration. A peak at 889-902 cm⁻¹ corresponds to TaO₆ octahedra units and Ta suboxides of the composites.³⁵ The CMT:Ta₂O₅ composites show similar vibration modes, it confirms the formation of tantalum oxide with that of CMTs.

XRD analysis

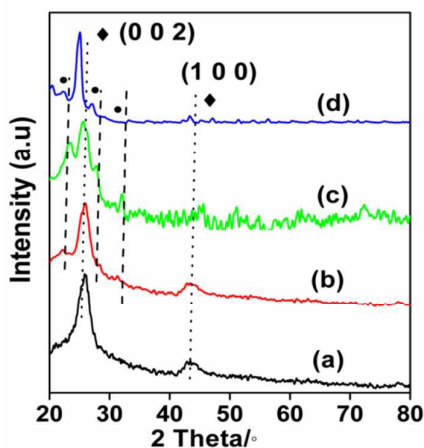


Fig. 4 Powder XRD patterns of the (a) CMTs (b) CMT:Ta₁ (c) CMT:Ta₂ and (d) CMT:Ta₃

The XRD patterns of CMTs, CMT:Ta₁, CMT:Ta₂ and CMT:Ta₃ were shown in the Fig.4. The peaks at 2-theta values of 25.9° and 43.5° with the (0 0 2) and (1 0 0) faces of graphite diffraction patterns respectively. This peaks are well matched with earlier literature values (JCPDS Card no: 23-64).^{8,18, 36-37} From the Fig. S1† the cotton XRD shows the higher intensity peak at 22.3° and low intensity peak at 15.9° suggests that morphological changes were observed during combustion process and XRD patterns of the cotton fiber and CMTs were not identical. The new peaks at 22.7°, 28.3° and 36.1° were due to the formation of Ta₂O₅ with carbon microstructures.³⁸ Hence the XRD studies confirmed the crystalline nature of micro tubes and CMT:Ta₂O₅ composites.

X-ray Photoelectron Spectroscopy (XPS) analysis

The XPS is powerful technique to investigate the electronic properties of species formed on the surface. XPS reveals the electronic environment, oxidation state, binding energy and spin multiplicity. The bonding properties can be influence the binding energy of the metal oxide composites. The XPS traces of CMTs and CMT:Ta₃ were shown in the Fig. 5. It reveals the presence of C, O and Ta. The XPS survey graphs of composites show a carbon signal (285.10 eV) for carbon 1s peak. The highly intense broad bands around 531 eV confirm the presence of oxygen atoms. The CMT:Ta₃. The C 1s, O 1s, Ta 4p and Ta 4f appear at 285.5, 531.2, 233.02 and 30 eV respectively.³⁹ Fig. 5(b) shows the peaks at 233.02 and 240.8 eV are related to Ta 4d_{5/2} and Ta 4d_{3/2} respectively. The peak fitting spectra of the Ta 4f for the composite shows the values at 25.8 eV and 30.04 eV for 4f_{7/2} and 4f_{5/2} eV respectively. The XPS survey graph of the parent CMT was given in the Fig.5a. It clearly suggests that presence of carbon elements. From Fig. 5b the Ta 4f core level spectra deconvoluted into the two peaks here tantalum 4f peak shows the higher binding energy value due to the formation of Ta₂O₅ with carbon microstructures. Fig 5d also shows the higher binding energy values for the 4p spectra, here 4p core spectra deconvoluted in the four peaks, but the two low intensity shake up satellite peaks resumes tantalum has suboxides, because Ta(V) may possess the various oxidation states. The O 1s core level XPS spectral traces show an asymmetric nature and the deconvoluted spectral trend suggesting that there is more than one type of oxygen atoms was bonded to Ta.⁴⁰ The O 1s peaks of the CMTs and CMT:Ta₃ XPS are shown in Fig.5(e) and (f) respectively. The deconvolution of O1s peak in to four peaks for CMT:Ta₃, but in case of the CMTs only two deconvoluted peaks was observed. Here the oxygen molecules binding energy more for the CMT:Ta₃, when compared to CMTs. The CMT:Ta₃ exhibit the peaks at 533.4, 531.8, 530.1 and 529.2 eV for the Ta-OH, Ta=O, Ta-O, Ta-O and Ta-O(H₂O) respectively.⁴¹ It indicate the tantalum has +5 oxidation state (Ta⁺⁵) and tantalum present in the form of oxides and sub oxides. In this O1s spectra the presence of 533.4 eV, ascribed to oxygen coupled to the hydroxyl or hydrated molecules. The CMT:Ta₂O₅ composites may contains O-H groups. It has been consistent with the FTIR

and DRS results. The XPS spectral analysis also confirm the formation of Ta_2O_5 for the CMT: Ta_2O_5 composites and tantalum in +5 oxidation state and stability of the composites.

FESEM and TEM analysis

The microscopic analysis is an evidence for the formation of microtubes during combustion of cotton fibers. The fiber sheets will be twisted by self rolling process at 450 °C. The twisting of the sheets will be depending on the direction and density of oxygen. Fig.6a confirms the CMTs formation and the outer diameter from 2 to 5 μ and length in mm.^{42,43} From Fig. 6d & 6g also shows the Ta_2O_5 formed evenly on the surfaces of CMTs. The microtube nature was not changed during the formation of CMT: Ta_2O_5 composite. The TEM image and

SAED patterns of CMTs and CMT: Ta_2O_5 was given Fig. 6(b&c, e&f, h&i). This clearly suggests that the crystalline nature of CMTs with stable confinements.⁴⁴ The FESEM analysis is evidence for the formation of CMTs.

The FESEM/TEM/EDAX (Fig. S2, S3&S4†) of the CMTs and CMT: Ta_2O_5 clearly suggest the presence of carbon and oxygen for CMTs, where as CMT: Ta_1 composite have Ta, C and O. Silica also present in negligible traces. The electron microscopy study confirms that the microtube formation at optimized condition, crystallinity was not change during the formation of CMTs and tantalum oxide composites. Hence, oxygen only play key role in the formation of CMTs.

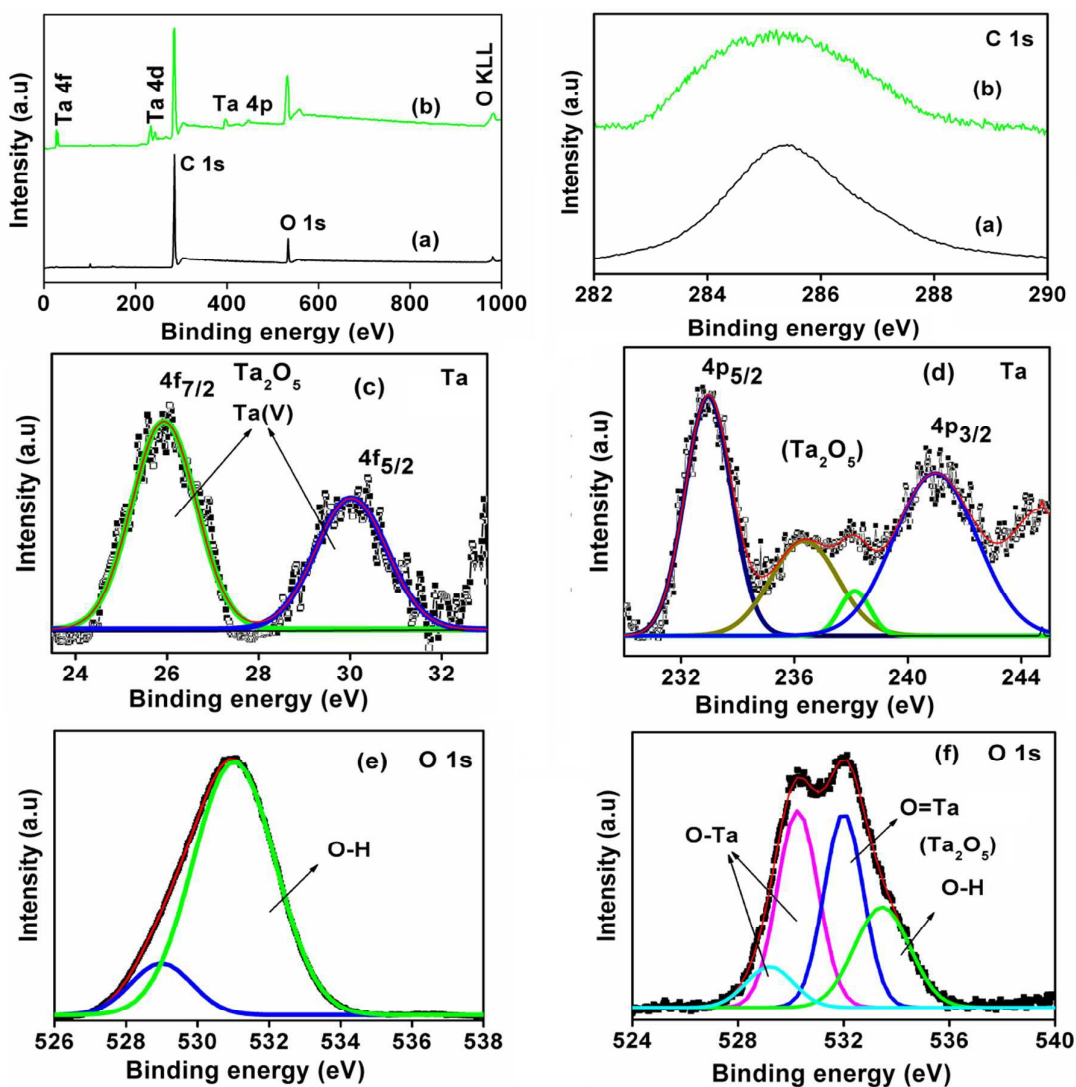


Fig. 5 XPS curves of the survey and C 1s spectra of the (a) CMTs and (b) CMT: Ta_3 ; (c) Ta 4f spectrum and (d) Ta 4p spectrum of the CMT: Ta_3 composites; (e) O 1s spectrum of CMTs and (f) CMT: Ta_3 composites.

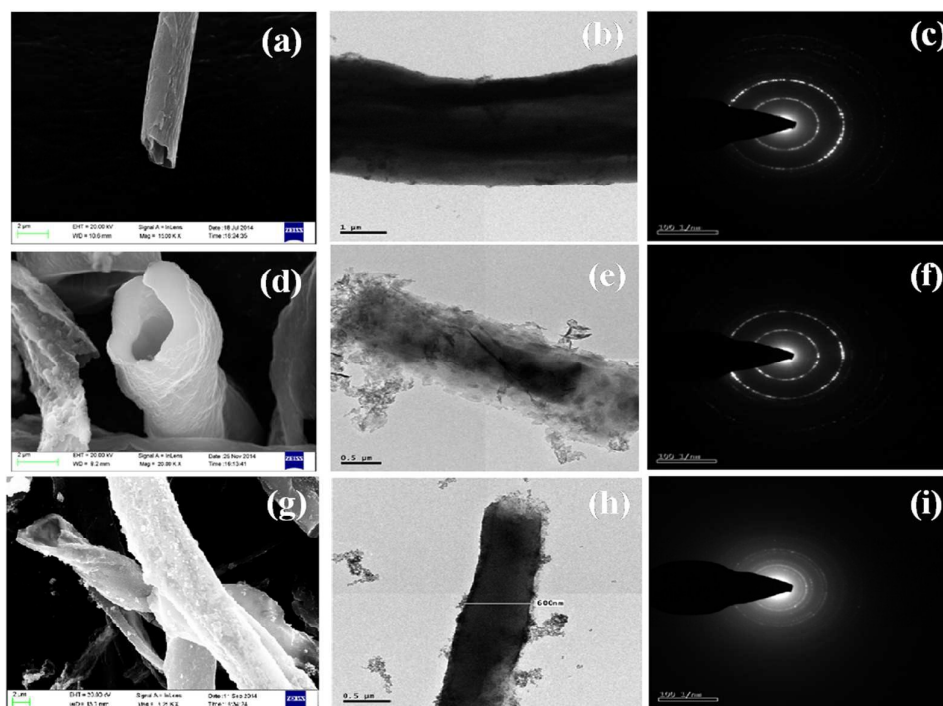


Fig. 6 FESEM images of the (a) CMTs (d) CMT:Ta₁ (g) CMT:Ta₃ and TEM images of (b) CMTs (e) CMT:Ta₂ (h) CMT:Ta₃ and SAED patterns of (c) CMTs (f) CMT:Ta₂ (i) CMT:Ta₃

Surface area measurements

The Brunauer-Emmett-Teller (BET) surface area and N₂-adsorption/desorption isotherms, and the pore volume studies for the CMTs, CMT:Ta₁, CMT:Ta₂, CMT:Ta₃ are given in Fig. 7. These composites have type-II isotherms, but a steep increase was observed above P/P₀ = 0.7. The BET surface area of the CMTs, CMT:Ta₁, CMT:Ta₂ and CMT:Ta₃ catalysts were determined to be 270, 223, 164 and 132 m²/gm respectively. The surface area values were reduced, it may be due to the formation of CMT:Ta₂O₅ composites. The pore size distribution curves of samples were evaluated from the adsorption branches of the isotherms and given in the Fig. S5†. The average pore diameter of CMTs, CMT:Ta₁, CMT:Ta₂ and CMT:Ta₃ is 22 Å, 19 Å, 21 Å and 14 Å. The BET data satisfactorily correlate with the XRD results and the discrepancy between BET and XRD data can be due to the complicated geometry of the polycrystalline nature of composites. Hence, the surface area was reduced gradually by increasing the tantalum oxide percentages, and the catalytic active site also been increased. Hence, the composite can behave as good surface active catalysts in oxidation reaction.

Particle size analysis

The CILAS particle size analyzer model 1180 was used to measure the particle size. Depending on the size of the particle, required quantity of CMTs was dispersed in ethanol for the particles of 1 μm size 0.05 gm sample is required and for larger particle (> 400 μm) around 5.0 gm of sample is required. To avoid the agglomeration of particles ultrasonic vibrator was switched on during the measurement. The suspension was pumped through a detector and a laser beam. The equipment analyzes the particle size and also the weight percent of the fraction. The histogram was shown in below Fig S6†. The diameter at 10%, the particle size was 5 μm, diameter at 50% the particle size was below 10 μm, diameter at 80% the particle size was at 20 μm, the mean diameter of the CMTs was 16 μm. Whereas the average particle size of the CMT:Ta₁, CMT:Ta₂ and CMT:Ta₃ are 17.5 μm, 19.8 μm and 23.5 μm respectively. The surface area was reduced while increase in particle size.

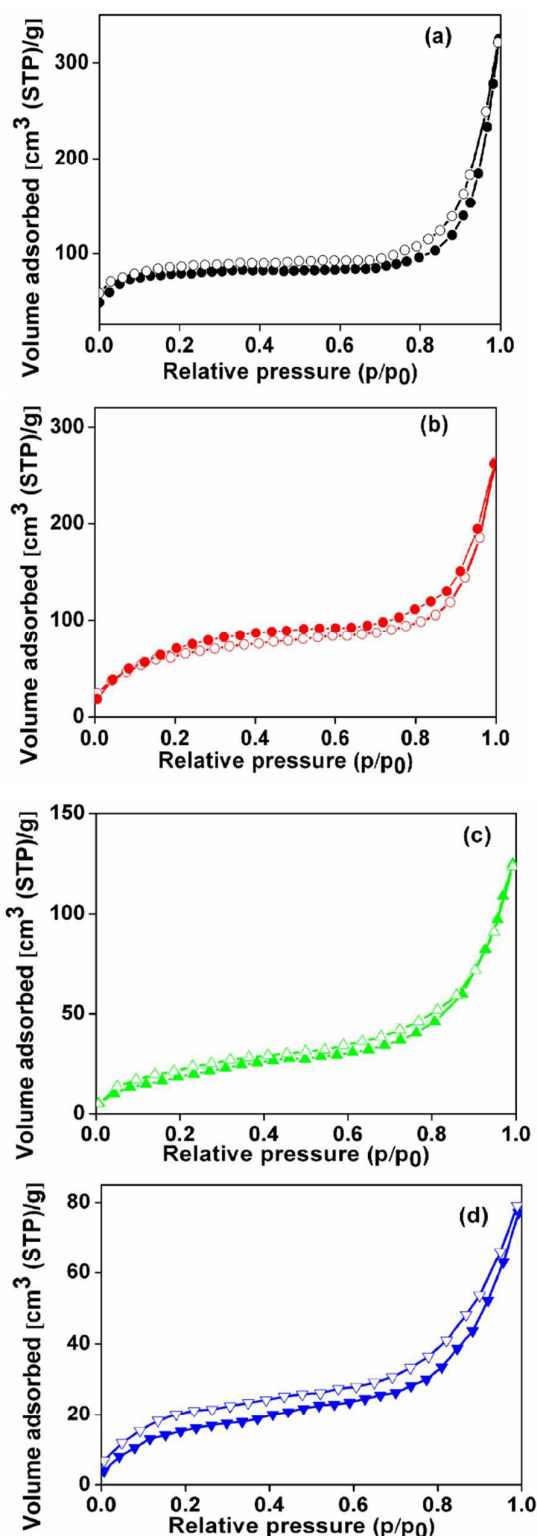


Fig. 7 N_2 -adsorption and desorption isotherms of the (a) CMTs (b) CMT:Ta₁ (c) CMT:Ta₂ and (d) CMT:Ta₃

Photocatalytic studies: Mechanistic issues involved in the removal of adsorbed the XO and MO dyes

The photocatalytic removal of the adsorbed XO and MO with CMTs, CMT:Ta₁, CMT:Ta₂ and CMT:Ta₃ under visible light irradiation has been studied. The removal percentages of the adsorbed dye and kinetic parameter were evaluated from the equation (1). The rate of reaction follows the first order rate equation.

$$\ln \left(\frac{C_t}{C_0} \right) = -k t \quad (2)$$

Here C_t is the concentration of the dye at different time, C_0 is the initial concentration, t is the time and k is the rate constant in min^{-1} .

The removal efficiency was calculated by optical absorption spectral analysis. The aliquot samples of the reaction medium were collected and the consequent absorption changes were recorded at 436 ± 2 nm for XO dye (464 ± 2 nm in case of MO). The spectral changes are given in Fig. S7&S8†. CMT:Ta₁, CMT:Ta₂ and CMT:Ta₃ has more degradation performance, when compared to CMTs. From Fig. 8(i&iii) the removal percentages of XO are 45%, 62%, 80% and 100% for the CMTs, CMT:Ta₁, CMT:Ta₂ and CMT:Ta₃ respectively, But in case of MO the percentages of removal are 11%, 38%, 66% and 100%. The active sites present in the catalyst ascertain the higher catalytic performance.

Surface area of the active catalysts and particle size of the photocatalysts also has an impact of photooxidation reactions. Here the gradual increase in the mean particle size with the decrease of surface area of active catalysts may lead to the induced charge transfer in HOMO-LUMO energy levels to retards electron-hole recombination. The reaction was carried out at fixed concentration of the all reactants. The catalytic reactions exhibit *pseudo*-first order kinetic parameters. Fig. 8(ii&iv) shows the negative slope in all cases. The rate constants of XO were 0.0055 min^{-1} , 0.0060 min^{-1} , 0.0081 min^{-1} and 0.025 min^{-1} for the CMTs, CMT:Ta₁, CMT:Ta₂ and CMT:Ta₃ respectively, In the case MO dye rate constants are 0.00009 min^{-1} , 0.0082 min^{-1} , 0.0087 min^{-1} and 0.0091 min^{-1} CMTs, CMT:Ta₁, CMT:Ta₂ and CMT:Ta₃ respectively. During the degradation under visible light the photo generated holes and e^- s may react with surface hydroxyl groups and adsorbed water or O_2 to generate the active oxidative ionic radicals ($O_2^{\cdot-}$ and $\cdot OH$) in the reaction medium. The tube form of the catalyst with active site also can be increase the activity, even the microtubes contains the active tantalum oxide species could do the active surface of the catalysts, here the visible light pass through the tubes degrade the dye

molecules faster than carbon nanospheres. The O_2^- and $\cdot OH$ radicals are very reactive and quickly oxidize organic species at the CMTs surface.^{45,46} The Lewis acid sites enhances the acidic nature of catalyst and formation of active radical limits the dye removal time.⁴⁷ Under visible light irradiation e^- are excited from the valence band to the conduction band of CMT:Ta₂O₅ catalysts and creating charge vacancy in h^+ in V.B. During degradation, the generation of the $\cdot OH$ radicals along with the formation of hydrogen peroxides increases the catalytic activity towards degradation of dyes.⁴⁸ The generated peroxy radicals react with oxides of Ta leading to the formation of nascent oxygen. This happens, when the reduction of Ta(V) to lower oxidation states. The resulting the highly active

oxygen for the degradation of XO and MO under visible light irradiation.⁴⁹ The pentavalent oxidation state of Ta provides multiple e^- to vary the electrical conductivity and more e^- generated and enhance the catalytic activity. The Ta⁺⁵ induced the formation of oxygen vacancy sites and tantalum oxide predominantly shows more acidic over redox behaviour. Hence, the active site present on the CMTs modified with highly conductive active tantalum oxides can be leads to the degradation of the organic pollutants.^{50,51} The proposed radical ion mechanism was shown Fig.9. The degradation of the enlisted organics to carbon dioxide, water, other less toxic minerals such as ammonia, nitrates and sulphates.⁵²⁻⁵⁵

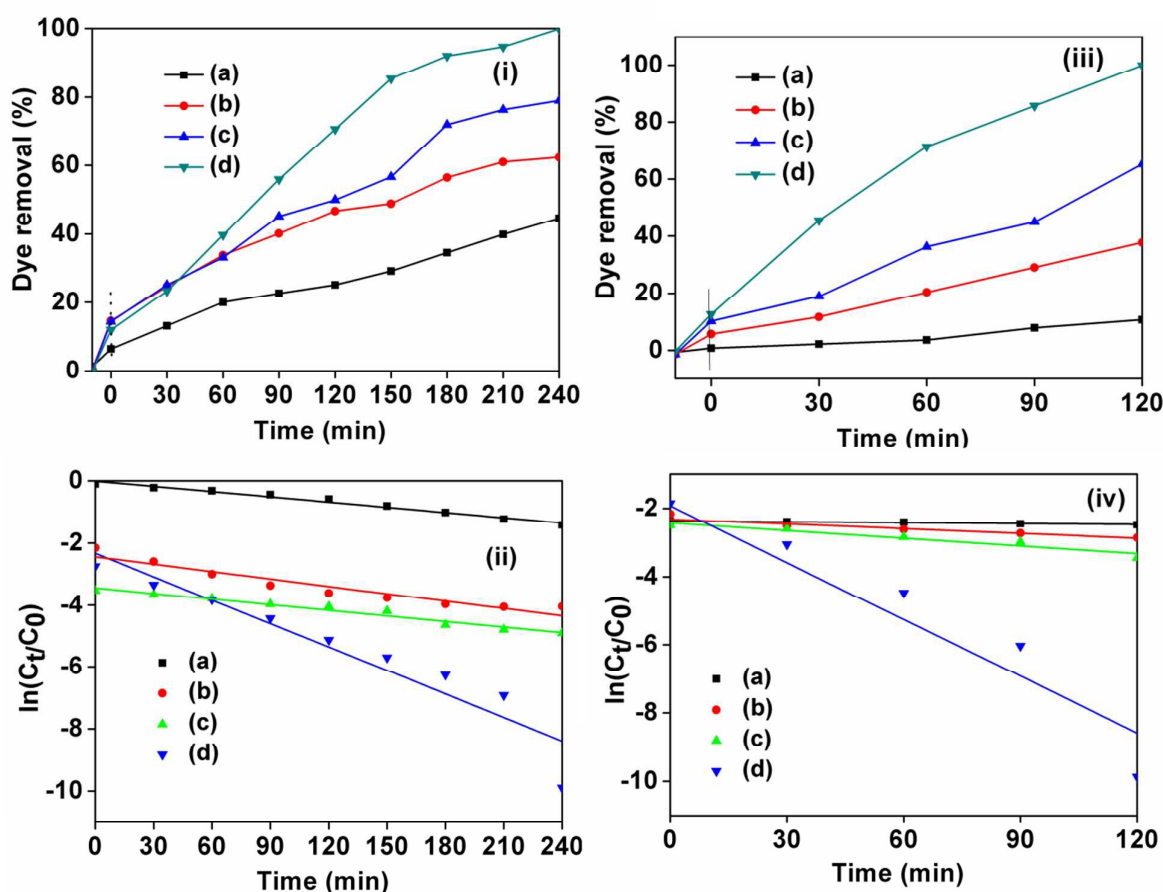


Fig. 8 The removal percentage of XO (i) and MO (ii) and the kinetic plots of XO (iii) and MO (iv); Here (a) CMTs (b) CMT:Ta₁ (c) CMT:Ta₂ and (d) CMT:Ta₃ composites.

The each recovered catalyst from the reaction was collected by nano-filtration and washed with the water, ethanol mixture and dried at 200 °C for 2 h. The extensively purified recovered catalysts were subjected to Raman spectra, powder XRD and DRS/UV-Visible spectra (Fig. S9-S12†). This spectral analysis confirms the stability

of the photocatalyst. Thus recovered catalysts spectral data was provided in the supporting information. The overall percentage of the conversion for the adsorbed both orange dyes was studied in the three cycles and given in the Fig. 10. It reveals the degradation and

efficiency of the reused catalysts comparatively same as fresh catalyst.

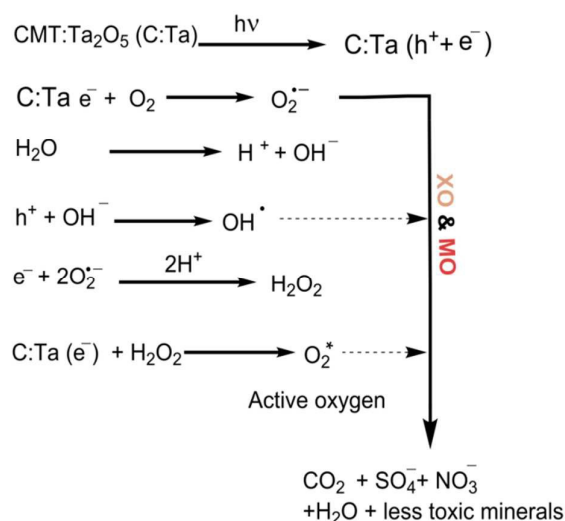


Fig. 9 The proposed radical-ions mechanism for the XO and MO degradation.

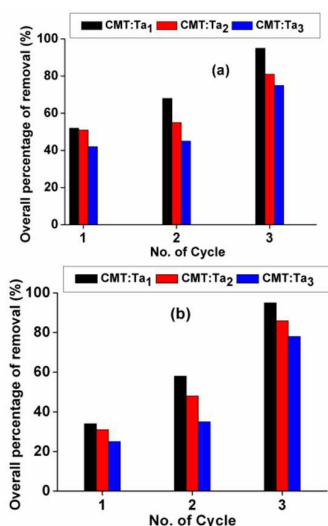


Fig. 10 Overall percentage of conversion for the recovered photocatalysts for the degradation of adsorbed (a) XO and (b) MO dyes

Conclusions

The novel economical production of CMTs was achieved in ambient conditions. The physico-chemical characterization also confirms the proposed differential aeration mechanism for the formation of CMTs. The microscopic and surface studies reveals the CMTs may be the promising materials in the field of catalysis and sustainable energy conversions. The CMT:Ta₂O₅ composite materials were synthesized by simple insitu method. The formation of CMTs and CMT:Ta₂O₅ composites were confirmed by the

FESEM, TEM, XPS, XRD analysis. The RAMAN, FTIR, DRS spectral data also reveals the formation of CMT/Ta₂O₅ composites. All the studies suggested that the stability and effective coupling of CMTs and Ta₂O₅. The composite materials were used as photocatalysts in the degradation of adsorbed XO and MO. The composites show higher photocatalytic activity and reused catalysts show comparable activity with fresh catalysts. This present investigation may leads to improve the research interest towards development low cost semiconducting materials by refractory metals for the sustainable energy conversions and environmentally eco-friendly materials for the catalysis. Hence visible light absorption these composites could be applicable as photocatalyst under visible light.

Acknowledgements

The authors are grateful to Ch Narendra reddy, post doctoral fellow, IICT-CSIR, Hyderabad, India, for his support during the experimental work. The authors are thankful to G. Bhaskar Raju, Chief Scientist, CSIR-NML Madras Complex, Chennai, India, for his support in surface area measurements. The authors are grateful to Col. Dr. Jeppiaar, Chancellor of Sathyabama University and Dr. T. Sasipraba, Dean, Sathyabama University, Chennai, India, for their constant support.

References

- H. Peng, Y. T. Zhu and D. E. Peterson, Q. Jia, *US Patent* 7,959,889, B2, 2011.
- R. Bacon, *J. Applied Phys.*, 1960, **31**, 283.
- H. B. Haanstra, W. F. Knippenberg and G. Verspui, *J. Crystal Growth*, 1972, **16**,71.
- S. Paul and S. K. Samdarshi, *New Carbon Mater*, 2010, **25**, 321.
- M. C. Yang and D. G. Yu, *J. Appl. Polym. Sci.* 1998, **68**, 1331.
- Y. Ma, J. Zhao, L. Zhang, Y. Zhao, Q. Fan, X. Li, Z. Hu and W. Huang, *Carbon*, 2011, **49**, 5292.
- G. Wen, H. Yu and X. Huang, *Carbon*, 2001, **49**, 4059.
- X. R. Wang, X. Zhao, J. Yanf, C.H. Lu and X.W. Du., *Carbon*, 2009, **47**, 1877.
- H. H. Nersisyan, T. H. Lee, K. H. Lee, D. Y. Maeng and J. H. Lee, *Mater. Lett*, 2013, **107**, 79.
- F. M. Morales, D. Mendez, Teresaben, S. I. Molina, D. Araujo and R. Garcia, *Microchim. Acta*, 2004, **145**, 129.
- N. A. Kiselev, J. L. Hutchison, A. P. Moravsky, E. V. Rakova, E. V. Dreval, C. J. D. Hetherington, D. N. Zakharov, J. Sloan and R. O. Loutfy, *Carbon*, 2004, **42**, 149.

- 12 Y. W. Ma, C. Y. Xiong, W. Huang, J. Zhao, X. A. Li, Q. L. Fan and W. Huang, *Chinese J. Inorg. Chem*, 2012, **28**, 546.
- 13 H. Yu, X. Huang, G. Wen, B. Zhong and L. Xia, *Mater. Lett*, 2011, **65**, 2004.
- 14 J. Libera and Y. Gogotsi, *Carbon*, 2001, **39**, 1307.
- 15 Y. Wei, *Chem. Lett*, 2014, **43**, 216.
- 16 M. Mecklenburg, A. Schuchardt, Y. K. Mishra, S. Kaps, R. Adelung, A. Lotnyk, L. Kienle and K. Schulte, *Adv. Mater*, 2012, **24**, 3486.
- 17 K. Kumar, B. Nandan, P. Formanek and M. Stamm, *J. Mater. Chem*, 2011, **11**, 10813.
- 18 V. A. Voloshin, V. G. Butko, A. A. Gusev and T. N. Shevtsova, *Phys. Solid State*, 2006, **45**, 392.
- 19 M. Baltes, A. Kytokivi, B. M. Weckhuysen, R. A. Schoonheydt, P. Vandervoort and E. F. Vansant, *J. Phy. Chem B*, 2001, **105**, 6211.
- 20 M. Shalom, M. Guttentag, C. Fettkenhauer, S. Inal, D. Neher, A. Llobet and M. Antonietti, *Chem. Mater*, 2014, **26**, 5812.
- 21 D. Nawn, D. Banerjee and K. K. Chattopadhyay, *Diamond Related Mater*. 2013, **34**, 50.
- 22 L. C. Jiang and W. D. Zhang, *Electrochimica Acta*, 2010, **56**, 406.
- 23 Q. L. Zhu and Q. Xu, *Chem. Soc. Rev.*, 2014, **43**, 5468.
- 24 G. R. Reddy and K. Chennakesavulu, *J. Mole. Struct*, 2014, **1075**, 406.
- 25 Y. Yu, L. Gu, C. Zhu, P. Van Aken and J. Maler, *J. Am. Chem. Soc*, 2009, **131**, 15984.
- 26 V. Anjos and A. Arantes, *RSC Adv*, 2015, **5**, 11248.
- 27 S. S. Arbuj, U. P. Mulik and D.P. Amalnerkar, *Nanosci. Nanotechnol. Lett*, 2013, **5**, 968.
- 28 M. Tian, J. Wen, D. MacDonald, R.M. Asmussen and A. Chen, *Electrochem. Commun*, 2010, **12**, 527.
- 29 M. Ahmad, E. Ahmed, Z. L. Hong, W. Ahmed, A. Elhissi and N. R. Khalid, *Ultrason. Sonochem*, 2014, **21**, 761.
- 30 K. Chennakesavulu, M. M. Reddy, G. R. Reddy, A. M. Rabel, J. Brijitta, V. Vinita, T. Sasipraba and J. J. Sreeramulu, *J. Mole. Struct*, 2014, **1091**, 49.
- 31 Q. Shishun, F. Linfeng, Z. Ruzhong, W. Yu and Y. Wu, *J. Mater. Chem. A*, 2014, **2**, 8190.
- 32 X. Wang, X. Liu, L. Lai, S. Li, J. Weng, Z. Zhou, Q. Cui, X. Chen, M. Cao and Q. Zhag, *Adv. Funct. Mater*, 2008, **18**, 1809.
- 33 A. M. Prakash and L. Kevan, *J. Am. Chem. Soc*, 1998, **120**, 13148.
- 34 J. Li, X. Chen, M. Sun, X. Cui, *Mater. Lett*, 2013, **110**, 245.
- 35 A. Wojtaszek, M. Ziolek and F. Tielens, *J. Phys. Chem. C*, 2012, **116**, 2462.
- 36 N. Reddy and Y. Yang, *Bioresource technol*, 2009, **100**, 3563.
- 37 N. Shi, G. Yin, X. Wei, Z. Xu, *Carbon*, 2009, **47**, 527.
- 38 D. Gompel, M. N. Tahir, M. Panthofer, E. Mugnaioli, R. Brandscheid, U. Kolb, W. Tremel, *J. Mater. Chem. A*, 2014, **2**, 8033.
- 39 X. Wuhong, Z. Jiupeng, D. Yanbo and Li, YaO, *Appl. sur. sci*, 2011, **257**, 10725.
- 40 S. Chen, J. Yang, C. Ding, R. Li, S. Jin, D. Wang, H. Han, F. Zhang and C. Li, *J. Mater. Chem. A*, 2013, **1**, 5651.
- 41 R. V. Goncalves, R. Wojcieszak, P. M. Uberman, S. R. Teixeira and L. M. Rossi, *Phys. Chem. Chem. Phys*, 2014, **16**, 5755.
- 42 X. G. Chen, S. S. Lv, P. P. Zhang, J. P. Cheng, S. T. Liu and Y. Ye, *J. Magn. Magn. Mater*, 2012, **324**, 1745.
- 43 S. Lijima, *Nature*, 1991, **354**, 56.
- 44 W. Zhou, Y. Liu, J. Guo and P. Wu, *J. Alloys Compos*, 2015, **621**, 423.
- 45 G. R. Reddy, S. Balasubramanian and K. Chennakesavulu, *J. Mater. Chem. A*, 2014, **2**, 15598.
- 46 N. Her, J. S. Park, J. Yoon, J. Sohn, S. Le and Y. Yoon, *Ind. Eng. Chem. Res*, 2011, **50**, 6638.
- 47 M. Czaplicka, *J. Hazard. Mater*, 2006, **134**, 49.
- 48 M. Ziolek, I. Sobczak, P. Decyk and I. Wolski, *Catal. Commun*, 2013, **37**, 85.
- 49 T. M. Breault and B. M. Bartlett, *J. Phys. Chem. C*, 2013, **117**, 8611.
- 50 R. Li, X. Ren, H. M. Wei, X. Feng, Z. Lin, X. Li, C. Hu and B. Wang, *J. Mater. Chem: A*, 2014, **2**, 5724.
- 51 W. Cui, H. Wang, Y. Liang, B. Han, L. Liu and J. Hu, *Chem. Eng. J*. 2013, **230**, 10.
- 52 Y. Fu, H. Chen, X. Sun and X. Wang, *Appl. Catal: B*, 2012, **111-112**, 280-287.
- 53 S. Kuriakose, B. Satpati and S. Mohapatra, *Phys. Chem. Chem. Phys*, 2014, **16**, 12741.
- 54 W. Wu, C. Jiang, and V. A. L. Roy, *Nanoscale*, 2015, **7**, 38.
- 55 W. Wu, X. Xiao, S. Zhang, F. Ren, and C. Jiang *Nanoscale Res. Lett*. 2011, **6**, 533.